arXiv:1604.03254v1 [astro-ph.CO] 12 Apr 2016

Discovery of a Supercluster at $z \sim 0.91$ and Testing the ΛCDM Cosmological Model

Jae-Woo Kim[1,2], Myungshin Im[1,2], Seong-Kook Lee[1,2], Alastair C. Edge[3], Minhee Hyun[1,2], Dohyeong Kim[1,2], Changsu Choi[1,2], Jueun Hong[1,2], Yiseul Jeon[2], Hyunsung David Jun[2,4], Marios Karouzos[2], Duho Kim[2,5], Ji Hoon Kim[6], Yongjung Kim[1,2], Won-Kee Park[7], Yoon Chan Taak[1,2], and Yongmin Yoon[1,2]

kjw0704@gmail.com, mim@astro.snu.ac.kr

ABSTRACT

The ΛCDM cosmological model successfully reproduces many aspects of the galaxy and structure formation of the universe. However, the growth of large-scale structures (LSSs) in the early universe is not well tested yet with observational data. Here, we have utilized wide and deep optical–near-infrared data in order to search for distant galaxy clusters and superclusters ($0.8 < z < 1.2$). From the spectroscopic observation with the Inamori Magellan Areal Camera and Spectrograph (IMACS) on the Magellan telescope, three massive clusters at $z \sim 0.91$ are confirmed in the SSA22 field. Interestingly, all of them have similar redshifts within $\Delta z \sim 0.01$ with velocity dispersions ranging from 470 to 1300 km s^{-1}. Moreover, as the maximum separation is ∼15 Mpc, they compose a supercluster at $z \sim 0.91$, meaning that this is one of the most massive superclusters at this redshift to date. The galaxy density map implies that the confirmed clusters are embedded in a larger structure stretching over ∼100 Mpc. ΛCDM models predict about one supercluster like this in our surveyed volume, consistent with our finding so far. However, there are more supercluster candidates in this field, suggesting that additional studies are required to determine if the ΛCDM cosmological model can successfully reproduce the LSSs at high redshift.

Subject headings: galaxies: clusters: general — galaxies: high-redshift

1. INTRODUCTION

Under the currently popular ΛCDM cosmology (Im et al. 1997; Riess et al. 1998; Perlmutter et al. 1999; Eisenstein et al. 2005), the large-scale structure (LSS) of galaxies emerges when the initial density fluctuations grow with time through gravitational attraction between galaxies. The ΛCDM cosmological model has been successful in reproducing the LSS at $z \simeq 0$, showing the promise of the ΛCDM cosmology to explain our universe (e.g., Bahcall et al. 2003; Williamson et al. 2011; Benson et al. 2013).

However, the growth of LSSs has not been thoroughly tested yet with observational data at $z \gg 0$. LSSs stretch from several tens of Mpc to a few hundred Mpc, but there is a lack of data sets that are deep and wide enough to cover

[1]Center for the Exploration of the Origin of the Universe, Department of Physics and Astronomy, Seoul National University, Seoul 151-742, Republic of Korea

[2]Astronomy Program, FPRD, Department of Physics and Astronomy, Seoul National University, Seoul 151-742, Republic of Korea

[3]Department of Physics, University of Durham, South Road, Durham DH1 3LE, UK

[4]Jet Propulsion Laboratory, California Institute of Technology, 4800 Oak Grove Drive, Pasadena, CA 91109, USA

[5]Arizona State University, School of Earth and Space Exploration, P.O. Box 871404, Tempe, AZ 85287-1404, USA

[6]Subaru Telescope, National Astronomical Observatory of Japan, 650 North A'ohoku Place, Hilo, HI 96720, USA

[7]Korea Astronomy and Space Science Institute, Daejeon 305-348, Republic of Korea

such structures at high redshifts. So far, high-redshift LSS studies have been limited mostly to galaxy-cluster-scale structures ($\lesssim$1–2 Mpc), with mixed results. Some results show agreements with the ΛCDM cosmology models (Williamson et al. 2011; Bayliss et al. 2014), but others suggest too many massive clusters at $z \gtrsim 1$ (Jee et al. 2009; Gonzalez et al. 2012; Kang & Im 2015).

With the advance of large and deep imaging surveys, it is now possible to extend the test of the cosmological formation of LSSs to scales much larger than before. Specific predictions have been made about superclusters at high redshift. A supercluster represents the most massive structure in the universe with sizes of up to ∼100–200 Mpc, containing filaments, multiple galaxy clusters and groups. Several studies have pointed out that superclusters are useful objects to test cosmological models (Wray et al. 2006; Einasto et al. 2011; Lim & Lee 2014).

So far, only a handful number of superclusters have been found at $z \sim 1$. The Cl 1604 supercluster at z ∼0.91 has 8 member clusters and groups that have velocity dispersions in the range of ∼280 to 820 km s^{-1} (Lubin et al. 2000; Gal et al. 2008; Lemaux et al. 2012; Ascaso et al. 2014; Wu et al. 2014). Another supercluster is identified at $z \sim 0.89$ in the Elais-N1 field, containing 5 clusters (Swinbank et al. 2007). A compact supercluster, RCS 2319+00 (Gilbank et al. 2008), stands as the most massive supercluster found at z ∼0.9 with the summed mass of members exceeding $10^{15}\,M_{\odot}$ (Faloon et al. 2013), and a separation between the member clusters is less than 3 Mpc. Finally, the Lynx supercluster at $z \sim 1.26$ contains two X-ray clusters and three groups confirmed spectroscopically (Rosati et al. 1999; Mei et al. 2012).

In order to unveil LSSs and other interesting high-redshift objects, we have been conducting the Infrared Medium-deep Survey (IMS; Im, M., et al. 2016, in preparation). The IMS is a deep ($J \sim 23$ AB mag) and wide ($\sim$ 120 deg^2) near-infrared (NIR) imaging survey that combines deep J-band imaging data with other optical/NIR survey data, making it possible to find LSSs at $z \sim 1$. Here, we report the discovery of a new, massive supercluster at $z \sim 0.9$ in the SSA22 area as the first result, and discuss if such an LSS is compatible with cosmological simulation predictions.

We adopt cosmological parameters for the flat universe with Ω_m =0.27, H_0=71 km s^{-1} Mpc^{-1}, and σ_8 =0.8. All magnitudes are in the AB system. In addition, all distance scales are physical scales based on the angular diameter distance, unless otherwise noted.

2. DATA AND CLUSTER FINDING

2.1. *Photometric Catalog*

Our work is based on wide and deep data sets for the SSA22 field (α =$22^h17^m00^s$ and δ =00°20′00″) from the Canada-France-Hawaii Telescope (CFHT) Legacy Survey (CFHTLS[1]), the United Kingdom Infrared Telescope (UKIRT) Infrared Deep Sky Survey (UKIDSS; Lawrence et al. 2007) Deep eXtragalactic Survey (DXS; Edge et al. 2016, in preparation), and the IMS. Although UKIDSS DXS (J- and K-bands) and IMS mapped nearly the entire CFHTLS–W4 ($ugriz$-bands) area (25 deg^2), the effective area is ∼20 deg^2 after excluding regions such as halos and spikes of bright stars. The 80% point-source detection limits are $u^* \sim 25.2$, $g' \sim 25.6$, $r' \sim 25.0$, $i' \sim 24.9$, and $z' \sim 23.9$ for the CFHTLS[2], and $J \sim 23.7$ and $K \sim 23.2$ for UKIDSS DXS and IMS (Kim et al. 2011, 2015). Sources were detected using SExtractor (Bertin & Arnouts 1996) in dual mode, and the unconvolved J-band images were used for the detection and to measure the J-band total magnitude. In addition, 2″ diameter apertures were applied to PSF matched images to derive aperture magnitudes for the color measurement. For this work, we applied a magnitude cut of $J = 23.2$ that is the 90% point-source completeness limit of the J-band data. Photometric redshifts (z_{phot}) were derived using the *Le Phare* software (Arnouts et al. 1999; Ilbert et al. 2006) after training the data using spectroscopic redshifts with flags of 3, 4, 23, and 24 from the VIMOS VLT Deep Survey (VVDS; Le Fèvre et al. 2005; Garilli et al. 2008). A measured redshift accuracy (σ_{pz}) by the normalized median absolute deviation is $\Delta z/(1+z) = 0.038$, and the outlier fraction is <5%. Details of the procedures are described in Kim et al. (2015).

[1] http://www.cfht.hawaii.edu/Science/CFHTLS/

[2] http://terapix.iap.fr/

2.2. *Finding MSGs*

Using all objects in the photometric redshift catalog, we searched for massive structures of galaxies (MSGs, galaxy clusters and groups) between $z = 0.8$ and $z = 1.2$. After splitting galaxies into redshift bins from $z_{bin} = 0.8$ to $z_{bin} = 1.2$ with an increment of 0.02 and a bin size of $|z_{phot} - z_{bin}| < \sigma_{pz}(1 + z_{bin})$ based on the best-fit photometric redshift, the Voronoi Tessellation technique (Ebeling & Wiedenmann 1993; Soares-Santos et al. 2011) is applied to measure a local density ($\rho = 1/\mathrm{area_{cell}}$) for each galaxy, which is converted into the normalized cell density, δ ($= \rho/\rho_{\mathrm{median}}$). Galaxies are identified to be in an overdense region if its δ value is above a threshold, δ_{thres}, following the prescription described in Soares-Santos et al. (2011). The δ_{thres} values are determined for each redshift bin, and they are found to vary between $\delta = 1.9$ and 2.0. The threshold corresponds to approximately 4σ above the mean density, if we fit the δ distribution with a Gaussian function in linear scale at $\delta < 1$[3]. We group galaxies whose cells have $\delta > \delta_{\mathrm{thres}}$ and are adjacent to each other as a possible overdense area. Then, we classify the overdense area as an MSG candidate if it has a probability over 95% that the signal is not due to random fluctuations (Eq. (3) of Soares-Santos et al. 2011). The sky position of a MSG candidate is assigned as the coordinate of the galaxy with the highest density. Also, the redshift is taken to be the median redshift of its galaxies within 1 Mpc from the MSG candidate center. MSG candidates from different redshift bins are merged into a single candidate if the projected separation between them is less than 2 Mpc, and their redshift bins overlap with each other.

We estimated the fraction of bona fide member galaxies in this approach using a galaxy mock catalog of `GALFORM` (Cole et al. 2000; Merson et al. 2013). For this, we randomly scatter mock galaxy redshifts with σ_{pz} above, and then select galaxies with $|z_{phot} - z_{cen}| < \sigma_{pz}(1 + z_{cen})$ and within 1.0 and 1.5 Mpc radii from central galaxies of 346 massive halos at $0.85 < z_{cen} < 1.15$, where z_{cen} indicates the halo redshift. The average fractions of bona fide members among selected galaxies are 50% and 30% for 1.0 and 1.5 Mpc, respectively. Therefore, we select MSG candidates, only if they have at least 25 galaxies ($N_{1.5\mathrm{Mpc}} \geq 25$) within a 1.5 Mpc radius and the photometric redshift uncertainty and with $J < J^* + 1$ (where J^* is characteristic magnitude). In total, there are 691 MSG candidates.

In order to identify supercluster candidates, we count the number of MSG candidates within a 10 Mpc radius and the photometric redshift uncertainty from each MSG candidate. Then, supercluster candidates are chosen as a group of at least 10 MSG candidates. Through this process, we find two supercluster candidates at the median photometric redshift of $\sim$0.89 and another at $\sim$0.92.

[3]This constraint is adopted to avoid the contribution of LSSs.

3. CLUSTER CONFIRMATION

3.1. *IMACS Observation and Redshift Determination*

Multi-object spectroscopy was performed on 2014 September 23, using the Inamori Magellan Areal Camera and Spectrograph (IMACS) on the Magellan/Baade telescope in its f/2 mode of a field that covers a $27'.4$ diameter field of view at $\alpha = 22^h13^m08^s$ and $\delta = 00°40'24''$. Of supercluster candidates described in the previous section, we chose the target field due to its unusually high concentration in a small area: six prominent ($N_{1.5\mathrm{Mpc}} > 40$) and nine less significant ($N_{1.5\mathrm{Mpc}} < 40$) MSG candidates, within a photometric redshift range of $0.85 < z_{phot} < 0.96$. Slitlets were assigned to galaxies in prominent candidates first, and then to those in less significant candidates. In order to choose target galaxies for the spectroscopy, we used the probability distribution function (PDF) of photometric redshifts from the *Le Phare* software. The integrals of the normalized PDFs within the uncertainty range (σ_{pz}) from the candidate redshift were calculated as the probability for each galaxy belonging to the cluster (Brunner & Lubin 2000; Papovich et al. 2010; Brodwin et al. 2013). Galaxies with probabilities >0.5 were selected as potential members. Spectra of potential members were taken using the 200 lines mm^{-1} grism with the WB5600–9200 filter ranging from 5600Å to 9200Å. One slit mask was used for the observation with $1'' \times 6''$ slitlets. In total, 320 slitlets were assigned for galaxies including potential MSG members (80%) and field galaxies

(20%). The spectral resolution was $\lambda/\Delta\lambda$ ∼600. The total on-source integration time was 2.5 hours (30 minutes×5) under ∼0″.9 seeing.

We used the Carnegie Observatories System for MultiObject Spectroscopy (COSMOS[4]) to reduce the IMACS spectroscopic data. The procedure includes standard reduction algorithm, wavelength calibration, and sky subtraction. We extracted one-dimensional spectra for each source from two-dimensional spectra stacked by the COSMOS pipeline. The flux calibration was performed using an F5-type star that was also included in the slit mask.

The redshift of each galaxy was determined with the *SpecPro* software (Masters & Capak 2011). We mainly used the emission and absorption lines of [OII]3727, Ca H&K, the 4000Å break, the G-band, and the Balmer lines (Hδ and Hγ) for this. If only a single emission line was detected, we considered this as the [OII] line. If the identified line was not [OII], e.g., such as Hγ, Hβ, [OIII] or Hα, it would likely be accompanied by another line at shorter or longer wavelengths and be at a redshift that is difficult to explain the continuum shape (i.e., at a redshift that is very different from photometric redshifts). We successfully determined the redshift of 217 galaxies, implying a success rate of ∼70%. The success rate is ∼80% for galaxies at $i_{AB} \leq 22.5$. Among successful spectroscopic measurements, 51% comes from a single emission, and 7% comes from Ca H&K absorption lines.

3.2. *Discovery of Supercluster at* $z = 0.91$

Using the galaxies with spectroscopic redshifts, we determine the membership of each galaxy. For this process, we follow the iterative algorithm described in Lubin et al. (2002). First, we select galaxies within a 1 Mpc radius from the cluster position determined by the photometric redshift method in § 2.2. Then, we calculate the bi-weight mean (z_{cl}) and scale (σ_z) of redshifts of these galaxies (Beers et al. 1990). We exclude galaxies with $|z - z_{cl}| > 3\sigma_z$ or the relative rest-frame radial velocity greater than 3500 km s^{-1}. This process is repeated until no more galaxies are excluded. Finally, the dispersion (σ'_z) is calculated by the gapper method due to the small number of members and then converted into the velocity dispersion (σ_v). Uncertainties in σ_v are estimated by the Jackknife resampling. Through this process, we identify three galaxy clusters at $z \sim 0.91$ with $\sigma_v >$470 km s^{-1}, which corresponds to $M_{200} > 1.1 \times 10^{14} M_\odot$ at the cluster redshift (Carlberg et al. 1997; Demarco et al. 2010). Table 1 lists the properties of the confirmed clusters based on two different radii of 1 Mpc and 1.5 Mpc for the comparison. Independently, we estimated the uncertainty in σ_v by randomly selecting 100 times 11 and 7 spectroscopic members within a 1 Mpc radius of the centers of two galaxy clusters at $z \sim 1.2$ containing ∼20-30 galaxies each with σ_v =490-650 km s^{-1} (Muzzin et al. 2009). We find that the standard deviation from this exercise to be 160 km s^{-1} and 320 km s^{-1} for the 11 and 7 member cases, respectively, which are consistent with or smaller than the Jackknife resampling errors in Table 1.

Figure 1a shows example spectra of cluster members in the three confirmed clusters. Vertical lines indicate locations of [OII] (blue), Ca H&K (red), and Hδ (magenta) lines. Figure 1b displays the spectroscopic redshift distribution of confirmed members for each cluster. The fraction of members of which spectroscopic redshifts are determined by a single line is 55%, 29%, and 0% for IMSCl J2212+0045, IMSCl J2213+0052 and IMSCl J2213+0048, respectively. Note that the velocity dispersion based only on red galaxies could decrease as much as ∼50% of that from both blue and red galaxies (Gal et al. 2008). When we did a similar analysis on two clusters where at least 5 and 4 red galaxies ($(r-i) > 0.9$ and $(i-z) > 0.5$) are available (J2212+0045 and J2213+0048), σ_v becomes 200±149 and 1117±464 km s^{-1}, respectively. This suggests that the σ_v values in Table 1 could be overestimated. Figure 2 shows pseudo color images for the confirmed clusters with photometric (circles) and spectroscopic (squares) members.

For the SSA22 field, Durret et al. (2011) also identified candidate galaxy clusters using photometric redshifts derived from the optical CFHTLS data. Of our clusters, IMSCl J2213+0052 and IMSCl J2213+0048 have counterparts in their list, considering a matching radius of 3′ (∼1.5 Mpc at $z = 0.91$) and $\Delta z < 0.1$.

Interestingly, all the new clusters are massive

[4]http://code.obs.carnegiescience.edu/cosmos

and located at redshifts of z ∼0.908–0.920. In addition, the maximum projected angular separation between galaxy clusters is 16′.78, which corresponds to ∼15 Mpc (comoving) at the cluster redshift. The proximity of the three massive clusters suggests that this is a supercluster. Compared to galaxy clusters in the Cl 1604 supercluster with a maximum velocity dispersion of ∼800 km s^{-1}, the supercluster presented here may encompass one or more clusters that are more massive and is more comparable to the RCS 2319+00 supercluster members (710–1200 km s^{-1}) and members in the Elais-N1 field (660–1000 km s^{-1}). Additionally, the maximum projected angular separation is similar to that for the three most massive clusters in Cl 1604 (16′.24), larger than RCS 2319+00 (7′.62), and smaller than the Elais-N1 supercluster (32′.45). This new supercluster in the SSA22 field may be one of the most massive structures ever found at z ∼0.9. We summarize the properties of the known superclusters in Table 1.

4. DISCUSSION

4.1. *Large-scale Structure*

In order to see if there are more structures beyond the confirmed clusters through a galaxy density map, we apply the Voronoi tessellation technique described in § 2.2 to the redshift bin at $z = 0.914$, the mean redshift of the confirmed clusters. Then, we make a grid map with a grid cell size of 500 kpc across the entire SSA22 area and calculate the mean value of local densities (δ in § 2.2) for each grid.

Figure 3 shows the map of local densities at z ∼0.914 around the confirmed clusters over a 3.5 deg × 2.9 deg area (∼190 Mpc × 160 Mpc, comoving). Small and large red circles indicate the positions of the newly confirmed clusters and the IMACS pointing, respectively. Intriguingly, the density contours extend toward the south and northeast with the structure spanning from (R.A., decl.)=(333.12, -0.1) to (334.15, 1.5). The projected angular size of this structure is ∼114′.2 corresponding to ∼54 Mpc or ∼103 Mpc (comoving) at this redshift. We also overlay galaxies (orange points) with spectroscopic redshifts of $0.90< z_{spec} <0.92$ from the VVDS and the VIMOS Public Extragalactic Redshift Survey that are deemed reliable (flags 2–9 and 22–29; VIPERS; Garilli et al. 2014; Guzzo et al. 2014). Comparing the density map and the distribution of spectroscopic samples, it seems that the supercluster extends the northeast direction. Note that no spectroscopic redshifts are available in the southwest area. The density map suggests that the supercluster possibly extends to a much larger scale.

4.2. *Comparison with Models*

Here, we examine if the existence of the new supercluster at $z = 0.91$ can be explained with ΛCDM models.

First, we search for dark matter halos grouped similarly to our confirmed clusters from the Millennium simulation (Springel et al. 2005) with the WMAP-7 cosmology (Guo et al. 2013). We use 15 snapshots from $z = 1.77$ to $z = 0.51$, each with a 0.32 Gpc^3 cube (i.e., five times the volume of our data at $0.8 < z < 1.2$). At $z = 1.08$, the first structures with properties comparable to the new supercluster form, i.e., those containing at least three halos, each in excess of $M_{200} > 1.1 \times 10^{14} M_\odot$. Two such structures appear at this redshift. By $z = 0.8$, three or four such structures have formed. When translated to our survey volume, the simulation suggests ∼0.6–0.8 superclusters at $0.8 < z < 1.2$. If we use the Millennium simulation with $\sigma_8 = 0.9$, the number is comparable in this redshift range.

Second, we calculate the predicted number of superclusters based on the supercluster mass function of Lim & Lee (2014). As a conservative estimate, we set the supercluster mass at $10^{15} M_\odot$. Using their mass function at $z = 1$, the predicted number of superclusters with $> 10^{15} M_\odot$ in the 20 deg^2 area with $0.8 < z < 1.2$ is ∼0.6.

The expected numbers of superclusters from the models are consistent with the number of superclusters we identified so far. However, there are still two more supercluster candidates in the SSA22 field, and extended structures as discussed in § 4.1 may contain more superclusters. On the other hand, considering the uncertainty of cluster masses, the clusters can be lighter. If so, the observation and the model predictions can be reconciled since lighter superclusters are more abundant than heavier ones in models. To understand if there is any tension between observed superclusters and ΛCDM models, it is necessary to do a more thor-

ough analysis of larger cosmological simulations and an intensive spectroscopic mapping of these large structures.

Authors thank an anonymous referee for comments that were useful for improving the paper. This work was supported by the National Research Foundation of Korea (NRF) grant, No. 2008-0060544, funded by the Korea government (MSIP). ACE acknowledges support from STFC grant ST/L00075X/1. D.K. acknowledges fellowship support from the grant NRF-2015-Fostering Core Leaders of Future Program, No. 2015-000714, funded by the Korean government. M.H. acknowledges the support from Global PH.D Fellowship Program through the National Research Foundation of Korea (NRF) funded by the Ministry of Education (NRF-2013H1A2A1033110). We are grateful to UKIDSS team, the staff in UKIRT, Cambridge Astronomical Survey Unit and Wide Field Astronomy Unit in Edinburgh. The United Kingdom Infrared Telescope was run by the Joint Astronomy Centre on behalf of the Science and Technology Facilities Council of the U.K. This work is based in part on data products produced at the Canadian Astronomy Data Centre as part of the Canada-France-Hawaii Telescope Legacy Survey, a collaborative project of NRC and CNRS. This Letter uses data from the VIMOS Public Extragalactic Redshift Survey (VIPERS). VIPERS has been performed using the ESO Very Large Telescope, under the "Large Programme" 182.A-0886. The participating institutions and funding agencies are listed at http://vipers.inaf.it. This research uses data from the VIMOS VLT Deep Survey, obtained from the VVDS database operated by Cesam, Laboratoire d'Astrophysique de Marseille, France. Finally, authors also thank staff in the Las Campanas Observatory.

Facilities: Magellan (IMACS), UKIRT (WFCAM), CFHT.

REFERENCES

Arnouts, S.,Cristiani, S., Moscardini, L., et al. 1999, MNRAS, 310, 540

Ascaso, B., Lemaux, B. C., Lubin, L. M., Gal, R. R., Kocevski, D. D., Rumbaugh, N., & Squires, G. 2014, MNRAS, 442, 589

Bahcall, N. A., Dong, F., Hao, L., Bode, P., Annis, J., Gunn, J. E., & Schneider, D. P. 2003, ApJ, 599, 814

Bayliss, M. B., Ashby, M. L. N., Ruel, J., et al. 2014, ApJ, 794, 12

Beers, T. C., Flynn, K., & Gebhardt, K. 1990, AJ, 100, 32

Benson, B. A., de Haan, T., Dudley, J. P., et al. 2013, ApJ, 763, 147

Bertin, E., & Arnouts S. 1996, A&AS, 117, 393

Brodwin, M., Stanford, S. A., Gonzalez, A. H., et al. 2013, ApJ, 779, 138

Brunner, R. J., & Lubin, L. M. 2000, AJ, 120, 2851

Carlberg, R. G., Yee, H. K. C., & Ellingson, E. 1997, ApJ, 478, 462

Cole, S., Lacey, C. G., Baugh, C. M., & Frenk, C. S. 2000, MNRAS, 319, 168

Demarco, R., Wilson, G., Muzzin, A., et al. 2010, ApJ, 711, 1185

Durret, F., Adami, C., Cappi, A., et al. 2011, A&A, 535, 65

Ebeling, H., & Wiedenmann, G. 1993, Phys. Rev. E. 47, 704

Einasto, M., Liivamägi, L. J., Tago, E., Saar, E., Tempel, E., Einasto, J., MartínezV. J., & Heinämäki, P. 2011, A&A, 532, 5

Eisenstein, D. J., Zehavi, I., Hogg, D. W., et al. 2005, ApJ, 633, 560

Faloon, A. J., Webb, T. M. A., Ellinson, E., et al. 2013, ApJ, 768, 104

Gal, R. R., Lemaux, B. C., Lubin, L. M., Kocevski, D., & Squires, G. K. 2008, ApJ, 684, 933

Garilli, B., Guzzo, L., Scodeggio, M., et al. 2014, A&A, 562, 23

Garilli, B., Le Fèvre, O., Guzzo, L., et al. 2008, A&A, 486, 683

Gilbank, D. G., Yee, H. K. C., Ellingson, E., Hicks, A. K., Gladders, M. D., Barrientos, L. F., & Keeney, B. 2008, ApJ, 677, L89

Gonzalez, A. H., Stanford, S. A., Brodwin, M., et al. 2012, ApJ, 753, 163

Guo, Q., White, S., Boylan-Kolchin, M., De Lucia, G., Kauffmann, G., Lemson, G., Li, C., Springel, V., & Weinmann, S. 2013, MNRAS, 428, 1351

Guzzo, L., Scodeggio, M., Garilli, B. R., et al. 2014, A&A, 566, 108

Ilbert, O., Arnouts, S., McCracken, H. J., et al. 2006, A&A, 457, 841

Im, M., Griffiths, R. E., & Ratnatunga, K. U. 1997, ApJ, 475, 457

Jee, M. J., Rosati, P., Ford, H. C., et al. 2009, ApJ, 704, 672

Kang, E., & Im, M. 2015, JKAS, 48, 21

Kim, J. -W., Edge, A. C., Wake, D. A., & Stott, J. P. 2011, MNRAS, 410, 241

Kim, J. -W., Im, M., Lee, S. -K., et al. 2015, ApJ, 806, 189

Lawrence, A., Warren, S. J., Almaini, O., et al. 2007, MNRAS, 379, 1599

Le Fèvre, O., Vettolani, G., Garilli, B., et al. 2005, A&A, 439, 845

Lemaux, B. C., Gal, R. R., Lubin, L. M., et al. 2012, ApJ, 745, 106

Lim, S., & Lee, J. 2014, ApJ, 783, 39

Lubin, L. M., Brunner, R., Metzger, M. R., Postman, M., & Oke, J. B. 2000, ApJ, 531, L5

Lubin, L. M., Oke, J. B., & Postman, M. 2002, AJ, 124, 1905

Masters, D., & Capak, P. 2011, PASP, 123, 638

Mei, S., Stanford, S. A., Holden, B. P., et al. 2012, ApJ, 754, 141

Muzzin, A., Wison, G., Yee, H. K. C., et al. 2009, ApJ, 698, 1934

Merson, A. I., Baugh, C. M., Helly, J. C., et al. 2013, MNRAS, 429, 556

Papovich, C., Momcheva, I., Willmer, C. N. A., et al. 2010, ApJ, 716, 1503

Perlmutter, S., Aldering, G., Goldhaber, G., et al. 1999, ApJ, 517, 565

Riess, A. G., Filippenko, A. V., Challis, P., et al. 1998, AJ, 116, 1009

Rosati, P., Stanford, S. A., Eisenhardt, P. R., Elston, R., Spinrad, H., Stern, D., & Dey, A. 1999, AJ, 118, 76

Soares-Santos, M., de Carvalho, R. R., Annis, J., et al. 2011, ApJ, 727, 45

Springel, V., White, S. D. M., Jenkins, A., et al. 2005, Nature, 435, 629

Swinbank, A. M., Edge, A. C., Smail, I., et al. 2007, MNRAS, 379, 1343

Williamson, R., Benson, B. A., High, F. W., et al. 2011, ApJ, 738, 139

Wray, J. J., Bahcall, N, A., Bode, P., Boettiger, C., & Hopkins, P. F. 2006, ApJ, 652, 907

Wu, P. -F., Gal, R. R., Lemaux, B. C., Kocevski, D. D., Lubin, L. M., Rumbaugh, N., & Squires, G. K. 2014, ApJ, 792, 16

This 2-column preprint was prepared with the AAS LaTeX macros v5.2.

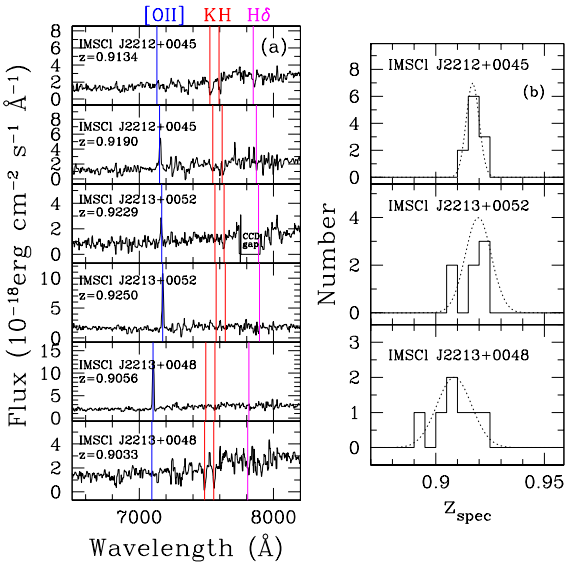

Fig. 1.— **(a)** Example IMACS spectra of the confirmed cluster members. The cluster IDs and the spectroscopic redshifts are noted in each panel. The vertical lines mark the [OII]3727, Ca H&K and Hδ4102 lines at the noted redshift. **(b)** Redshift distribution of spectroscopic members within 1 Mpc. The dotted lines show Gaussian distributions based on z_{cl} and σ'_z (see § 3.2 for details).

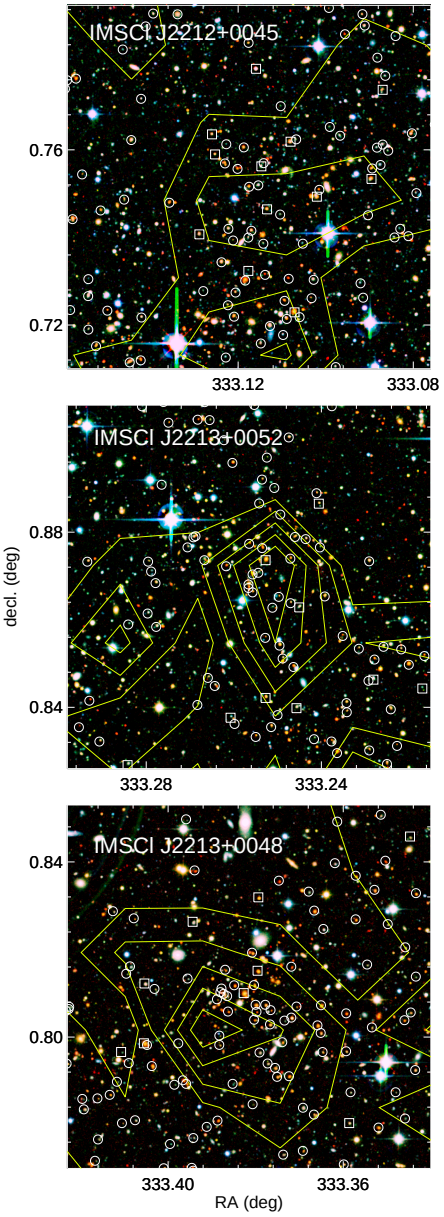

Fig. 2.— Pseudo-color images (giK-bands) of the confirmed clusters. These images were arbitrarily scaled for display purposes. The field of view is $5'\times5'$ corresponding to 2.4 Mpc×2.4 Mpc at the cluster redshift. The circles and the squares are for photometric and spectroscopic members, respectively. Yellow curves show contours for $<\delta>$=2, 4, 6, 7, and 10 at $z\sim0.91$ (§ 4.1).

Table 1: Summary of confirmed clusters in this study with applying two different radii (top) and previously reported superclusters at $z \sim 0.9$ (bottom).

Cluster	R.A. (J2000)	decl. (J2000)	Radius (Mpc)	$n_{\rm slit}$	$n_{\rm member}$	z_{cl}	σ_v (km s^{-1})	M_{200} ($\times 10^{14} M_\odot$)
IMSCl J2212+0045	22:12:28	00:45:06	1.0	19	11	0.9170±0.0008	474±152	$1.1^{+1.5}_{-0.8}$
			1.5	33	13	0.9171±0.0022	584±148	$2.1^{+2.0}_{-1.2}$
IMSCl J2213+0052	22:13:02	00:52:02	1.0	13	7	0.9196±0.0026	884±469	$7.2^{+18.7}_{-6.5}$
			1.5	26	9	0.9176±0.0028	944±305	$8.8^{+11.6}_{-6.1}$
IMSCl J2213+0048	22:13:31	00:48:42	1.0	17	7	0.9085±0.0041	1298±310	$23.0^{+20.7}_{-12.8}$
			1.5	25	11	0.9118±0.0036	1665±329	$48.5^{+34.8}_{-23.4}$

Supercluster	R.A.[a]	decl.[a]	z	$n_{\rm cluster}$	σ_v[b]	Size$_{\rm projected}$[b]	$< n_{\rm galaxy} >$[b]	Ref.
Cl 1604	16:04:23	43:13:08	0.85–0.94	8	688–818	$17'$	∼70	Wu+14[c]
					590–811		∼51	Gal+08[c]
Swinbank+07	16:08:27	54:35:47	0.89	5	730–1030	$32'$	∼11	Swinbank+07
RCS 2319+00	23:19:53	00:38:04	0.90	8	714–1202	$8'$	∼16	Faloon+13

[a] Coordinate for the most massive cluster.

[b] Values based on the three most massive clusters.

[c] Member galaxies within two times the virial radius in Wu et al. (2014) and 1 h^{-1}Mpc in Gal et al. (2008).

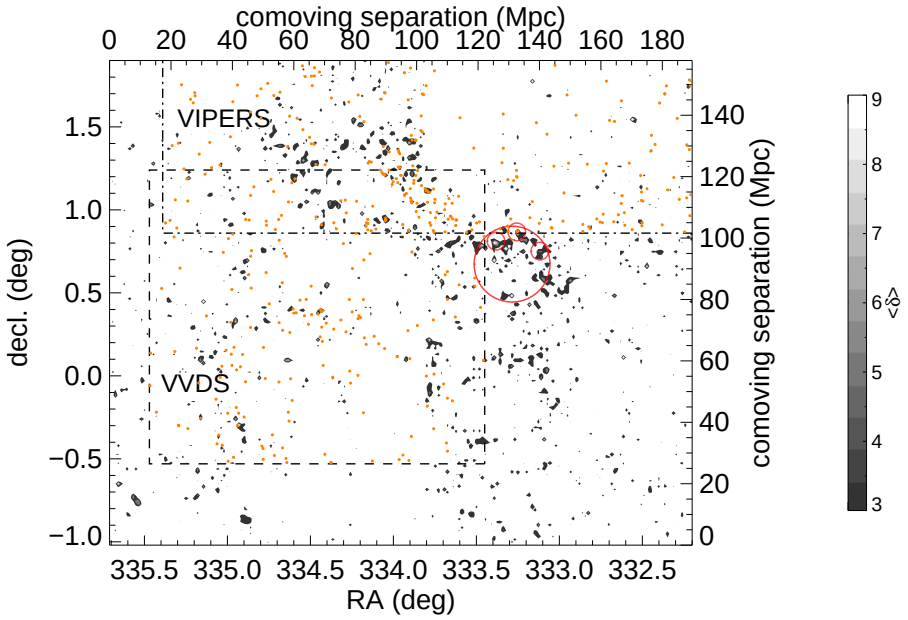

Fig. 3.— Overdensity contour at $z = 0.914$ around the confirmed clusters. Small and large red circles show the confirmed clusters and the IMACS field of view, respectively. Dashed and dotted-dashed boxes indicate survey boundaries of VVDS and VIPERS, respectively. The orange points are galaxies with spectroscopic redshifts between z =0.90 and 0.92 from VVDS and VIPERS. More MSG candidates exist at northeast of the supercluster, and spectroscopic samples from VVDS and VIPERS seem to connect the supercluster and the MSG candidates.